Supporting information:

Boron-doped porous Si anode materials with high initial Coulombic efficiency and long cycling stability

Ming Chen† [a, b], Bo Li† [a], Xuejiao Liu[a], Ling Zhou[a], Lin Yao[a], Jiantao Zai* [a], Xuefeng Qian* [a], and XiBin Yu* [b]

a Shanghai Electrochemical Energy Devices Research Center, School of Chemistry and Chemical Engineering and State Key Laboratory of Metal Matrix Composites, Shanghai Jiao Tong University, Shanghai, 200240, P. R. China.

*E-mail: xfqian@sjtu.edu.cn; zaijiantao@sjtu.edu.cn

b Education Ministry Key Lab of Resource Chemistry and Shanghai Key Laboratory of Rare Earth Functional Materials, Department of Chemistry, Shanghai Normal University, Shanghai 200234, China.

*E-mail: xibinyu@shnu.edu.cn

† These authors contributed equally to this work.

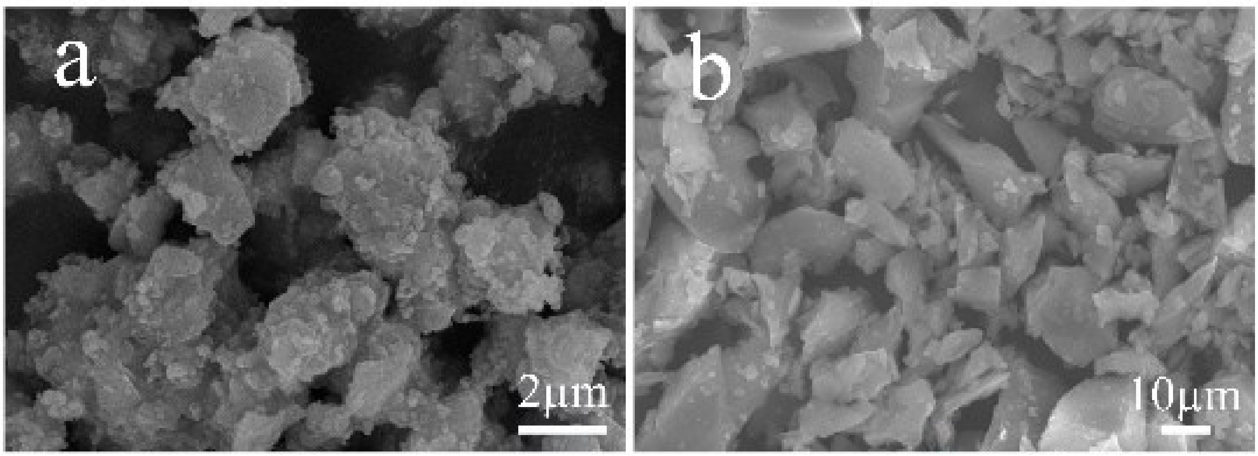

Fig. S1 SEM images of the size and morphologies of (a) ~2μm Si powders and (b) 200 mesh commercial Si powders.

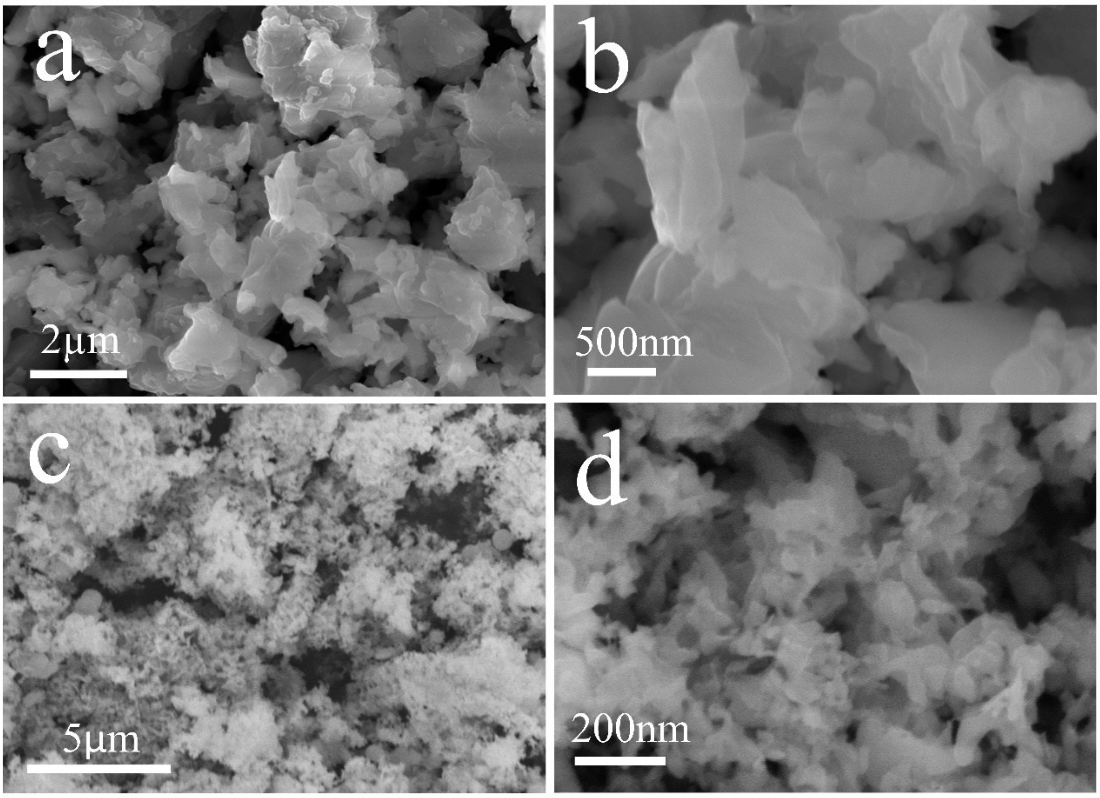

Fig. S2 SEM images of (a)-(b) as-prepared Mg_2Si, (c)-(d) pSi nanoplates from ~2μm Si powders as the raw material.

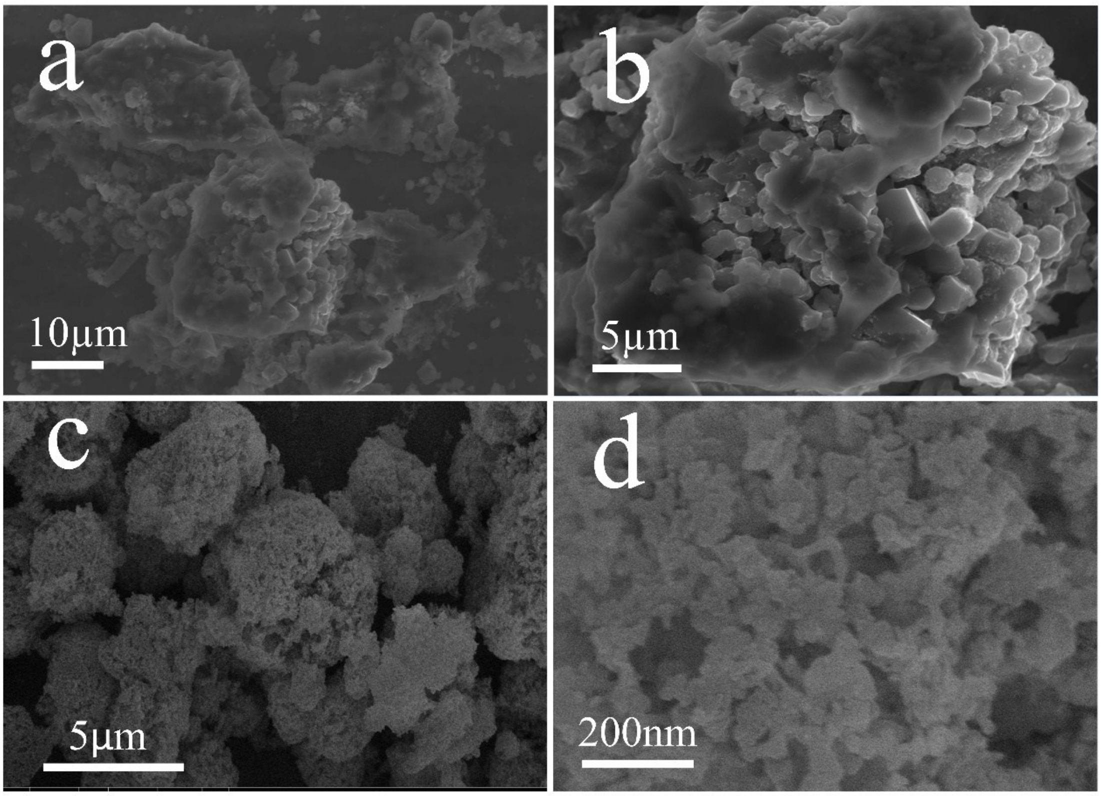

Fig. S3 SEM images of (a)-(b) as-prepared Mg_2Si, (c)-(d) pSi nanoparticles from 200 mesh commercial Si as the raw material.

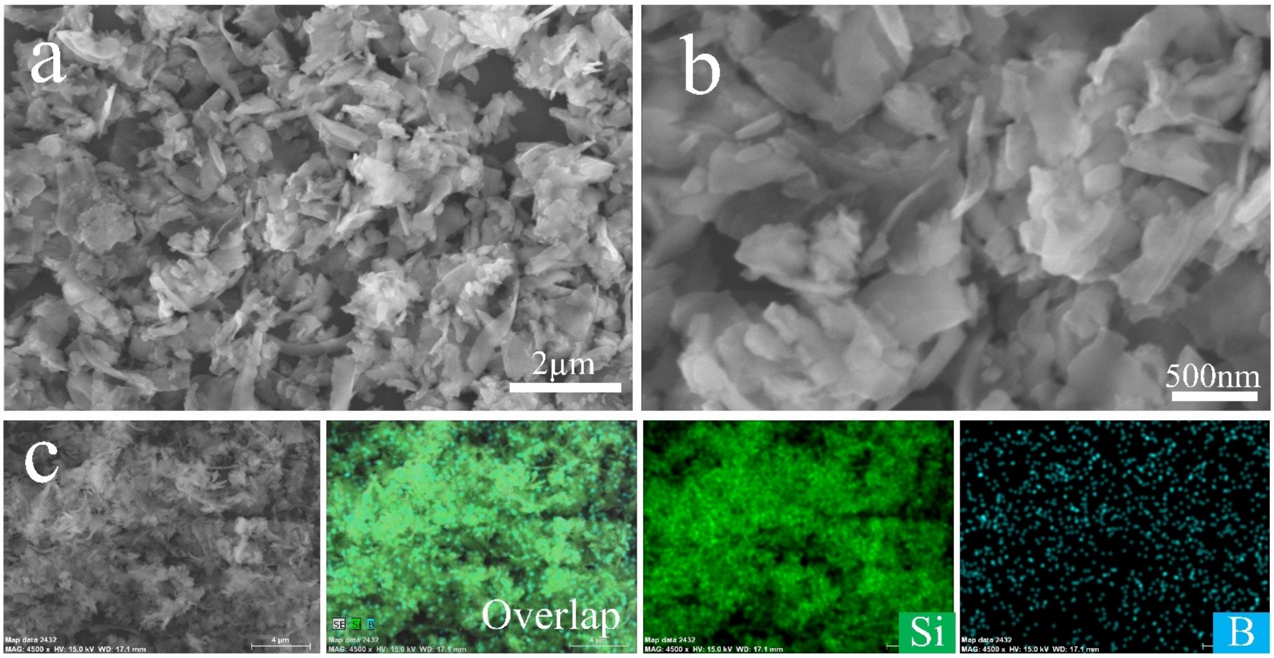

Fig. S4 SEM images of ~2μm B-doped Si powders milled from commercial p-type Si wafers and corresponding EDS elemental mapping images of Si (green) and B (blue).

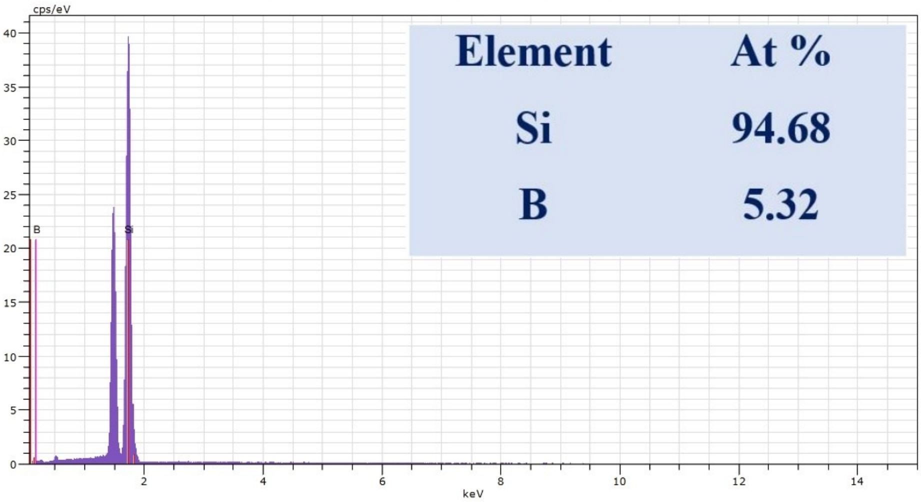

Fig. S5 EDS spectrum of B-doped porous Si material.

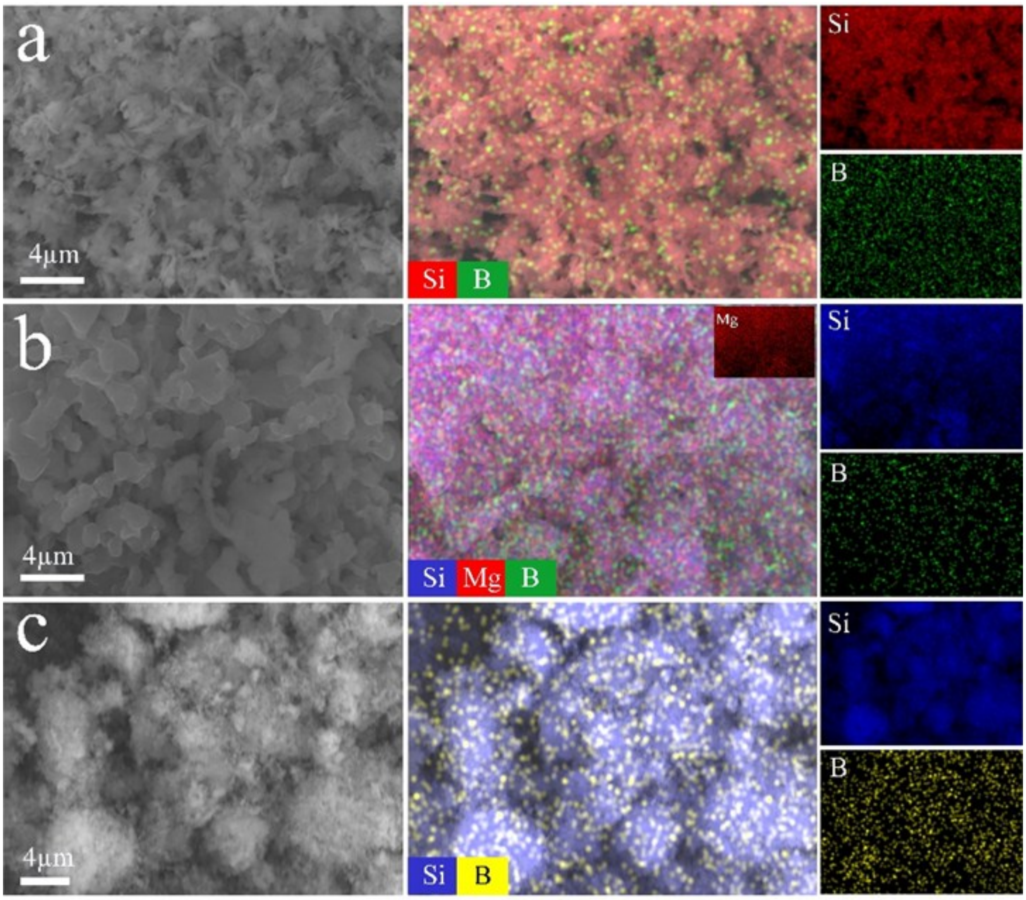

Fig. S6 EDS mapping images of ~2 μm B-doped Si powders milled from commercial p-type Si wafers (a), the intermediate product of B-doped Mg_2Si alloys (b) and B-doped porous Si material (c).

The B element of B-doped porous Si material (Fig. S6 c) originates from the raw commercial B-doped Si wafers (p-type Si wafers) (Fig. S6 a). After alloying and air-oxidation process of B-doped Si powders, B element is still kept which can be confirmed by EDS (Fig. S6).

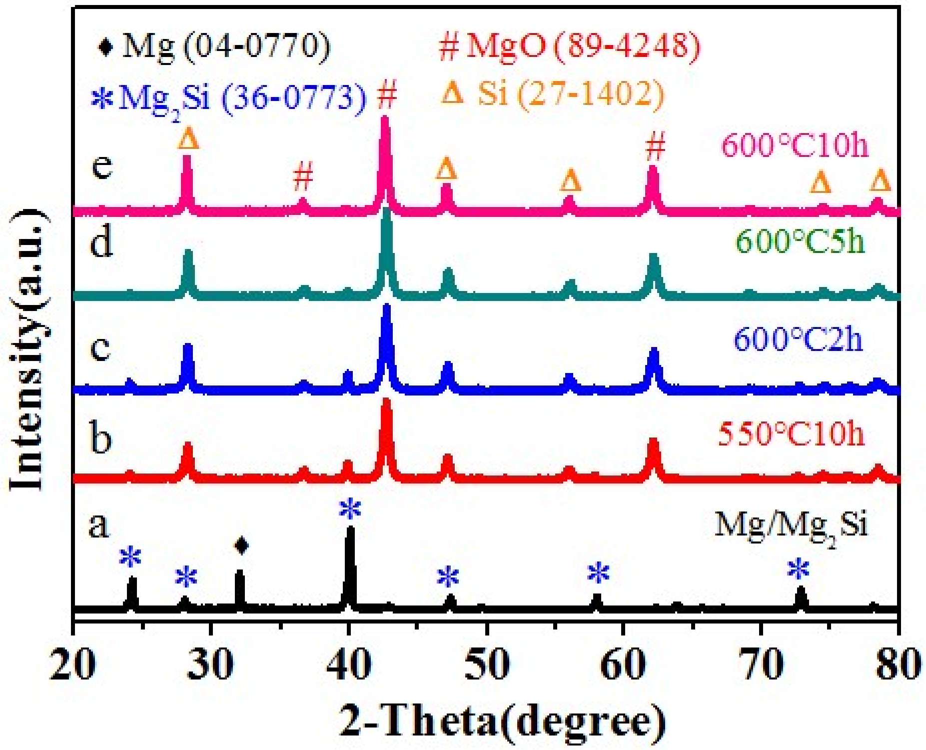

Fig. S7 XRD patterns of (a) Mg_2Si/Mg powder, and the as-prepared samples after the air-oxidation process at (b) 550℃ for 10 h, (c) 600℃ for 2 h. (d) 600℃ for 5 h. (e) 600℃ for 10 h.

Fig. S7 shows the appropriate temperature for the oxidation of Mg_2Si to Si, a series of related experiments concerning the heating of as-prepared Mg_2Si/Mg in air was carried out at temperatures of 550℃ and 600℃. Besides, we set the time of air oxidation of as-prepared Mg_2Si/Mg at 600℃ for 2 h,5 h and 10 h. The products obtained at 600℃ for 5 h, indicating that Mg_2Si can be completely transformed to Si without needing 10 h.

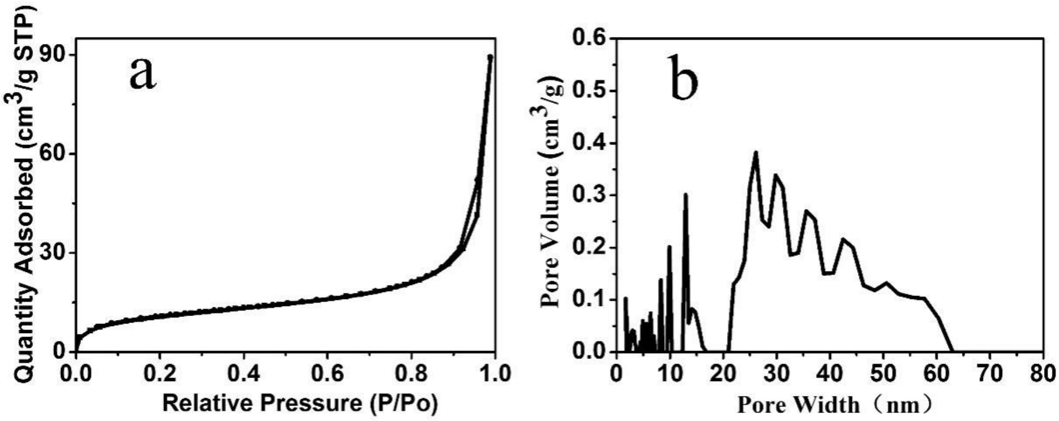

Fig. S8 (a) Nitrogen adsorption-desorption isotherm curves (b) BJH pore diameter distribution of pSi sample.

The porous structures of pSi sample were verified by nitrogen adsorption-desorption isotherm curves (Fig. S8). BET surface area of pSi samples is 32 $m^2 g^{-1}$ and the pore size of porous Si material is range from 2 to 60 nm revealing its hierarchical pore structure.

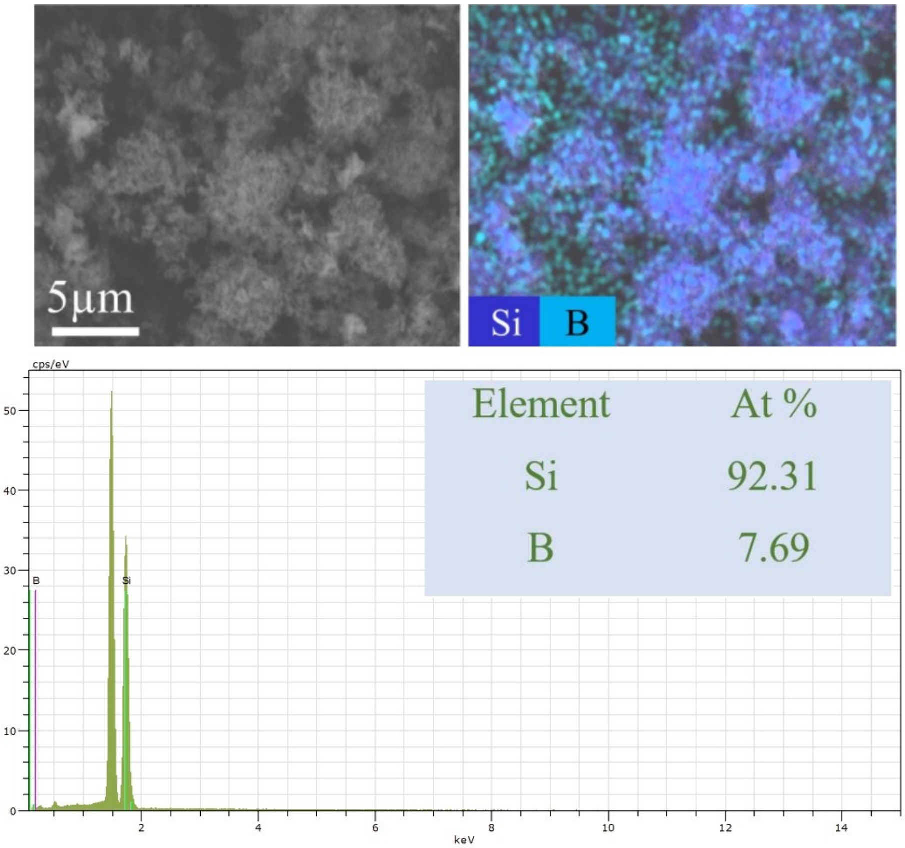

Fig. S9 EDS mapping and spectrum of HB-doped porous Si material.

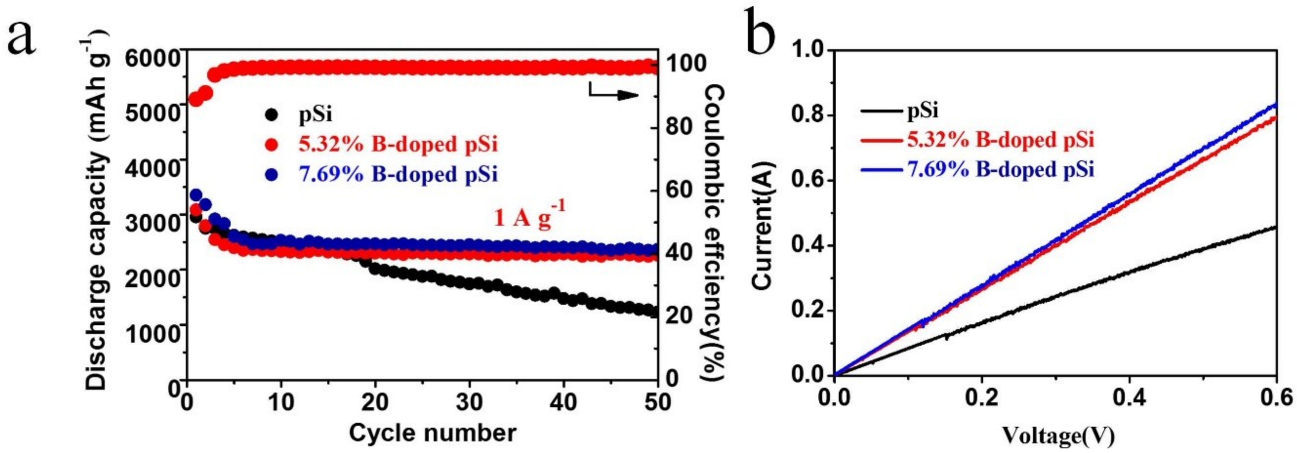

Fig. S10 (a) Cycling performances of porous Si and B-doped porous Si (5.32% and 7.69% of B) electrodes at 1 A g^{-1}. (b) I-V curves of porous Si and B-doped porous Si (5.32% and 7.69% of B) powders at 10 mV/s.

The conductivity and electrochemical performances of porous Si with different contents of B are studied (Fig. S10). Compared to undoped porous Si electrode, doping B can effectively improve the conductivity, capacity and stability of porous Si electrodes. However, doping more B (e.g 7.69%) can not effectively improve the conductivity and electrochemical performances of porous Si.

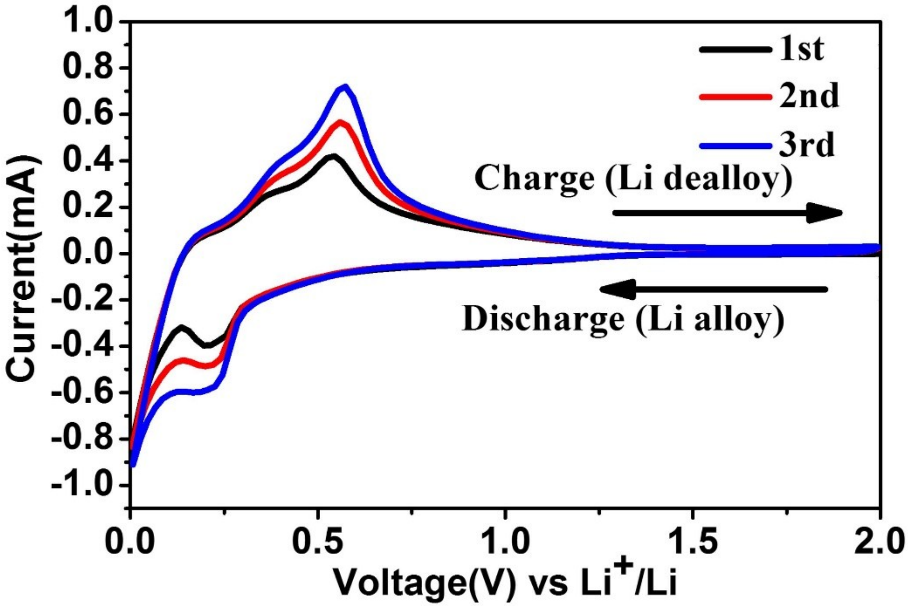

Fig. S11 Cyclic voltammetry (CV) curves of B-doped pSi electrode.

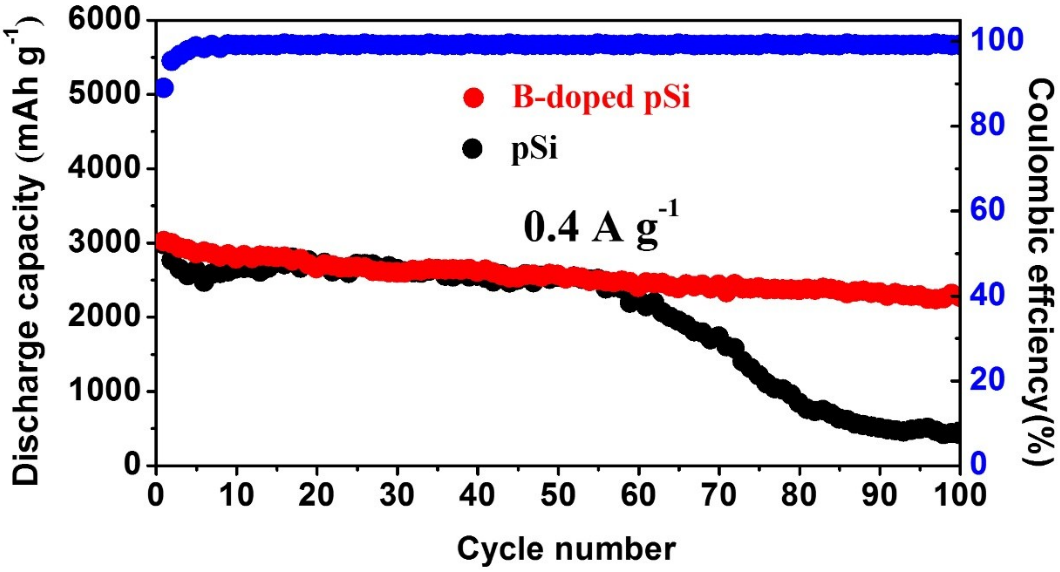

Fig. S12 Cycling stability of B-doped porous Si and undoped porous Si electrodes at 0.4 A g^{-1}**.**

Cycling performances of the B-doped porous Si and undoped porous Si electrodes at 0.4A g^{-1} are shown in Fig. S12. The initial discharge capacities of the B-doped porous Si and undoped porous Si electrodes are of 3016 and 2974 mAh g^{-1}, which correspond to reversible capacities of 2232 mAh g^{-1} and less than 500 mAh g^{-1} after 100 cycles.

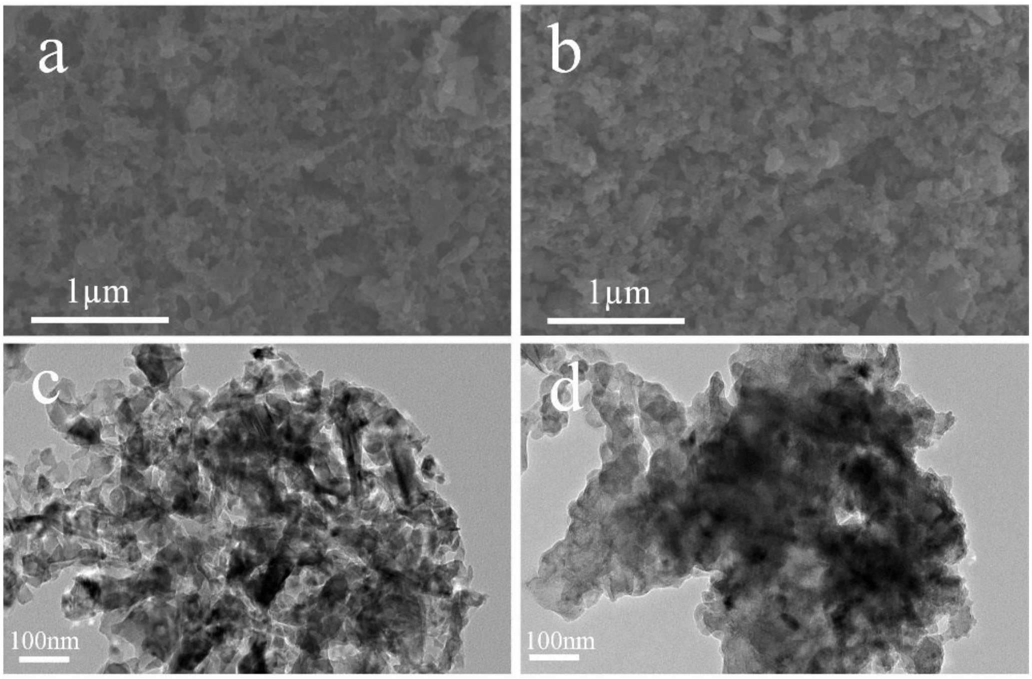

Fig. S13 SEM images of B-doped porous Si electrodes before (a) and (b) after 100 cycles and TEM images of B-doped porous Si materials before (c) and (d) after 100 cycles.

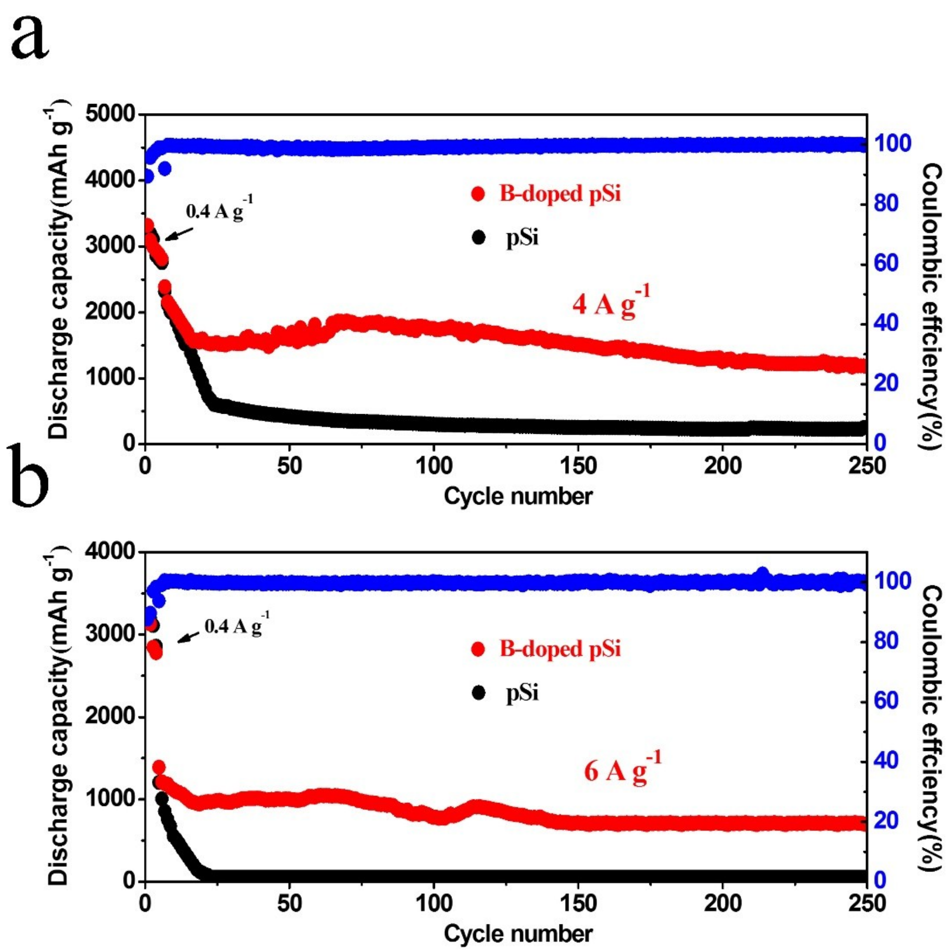

Fig. S14 Long-term cycling stability of B-doped porous Si and undoped porous Si electrodes at 4 A g^{-1} (a) and 6 A g^{-1} (b), respectively (the first three cycles at 0.4 A g^{-1}).

Long-term cycling stability of B-doped porous Si at higher current densities (Fig. S14) is studied. B-doped porous Si electrodes have a capacity of 1180 and 708 mAh g^{-1}at the current densities of 4 A g^{-1} and 6 A g^{-1} after 250 cycles, respectively. While the capacity of the undoped porous Si electrode is rapidly fading to 250 and 50 mAh g^{-1} at the current densities of 4 A g^{-1} and 6 A g^{-1} after 100 cycles. The results indicate the doped B can effectively improve the long-term cycling stability of Si electrodes at higher current density.